Journal of Inorganic and General Chemistry
ZAAC
Zeitschrift für anorganische und allgemeine Chemie
www.zaac.wiley-vch.de
RESEARCH ARTICLE
Check for updates
DOI: 10.1002/zaac.202200060

Synthesis and Structural Investigation of Protonated Haloacetyl Fluorides

Sebastian Steiner,[a] Christoph Jessen,[a] and Andreas J. Kornath*[a]

Dedicated to Prof. Dr. Wolfgang Beck on the Occasion of his 90th Birthday.

Herein, we report the *O*-monoprotonated species of chloroacetyl fluoride and fluoroacetyl fluoride in the binary superacidic systems HF/MF_5 and DF/MF_5 (M = As, Sb) as hexafluoridoarsenates and hexafluoridostibates. The colorless salts were characterized by low temperature vibrational spectroscopy, low temperature NMR spectroscopy and single-crystal X-ray diffraction. $[CClH_2C(OH)F][SbF_6]$ crystallizes in the monoclinic space group $P2_1/c$ with four formula units per unit cell and $[CH_2FC(OD)F][SbF_6]$ in the triclinic space group $P\bar{1}$ with two formula units per cell. The experimental data are discussed together with quantum chemical calculations at the ωB97XD/aug-cc-pVTZ-level of theory. Protonation leads to significant shortening of the C–F bond due to back-donation of fluorine lone-pair electrons.

Introduction

Protonation of weakly basic molecules and isolation as well as characterization of protonated, highly reactive intermediates is one of the fundamental targets in chemistry and essential for the understanding of reaction mechanisms, like in organic reactions or industrial superacidic catalysis.[1] For example, acyl fluorides are often used in Friedel-Crafts reactions and hence the introduction of the acyl moiety in molecules, especially due to their higher stability towards hydrolysis and, nevertheless, higher reactivity compared to other acyl halides.[2,3] Their properties, regarding reactions with strong Lewis acids such as SbF_5 or AsF_5 under formation of acylium salts, have been thoroughly investigated.[4–6] However, their Brønsted basicity and reactivity in superacidic media have not been examined comprehensively, yet. The smallest representative of this compound class is constituted by acetyl fluoride and its derivates. In 1969, *Olah et al.* investigated the properties of acetyl fluoride in the superacidic system HSO_3F/SbF_5 (*"magic acid"*) with NMR spectroscopy and was able to determine the acetylium ion but not the protonated species.[7] The chloroacetylium and fluoroacetylium ions were characterized by NMR spectroscopy by *Olah et al.* in 1975.[5] To the best of our knowledge, studies concerning haloacetyl fluorides in superacidic media and the influence of electron withdrawing groups on their basicity have not been reported so far. This prompted us to perform further investigations on acetyl fluoride and its halogenated derivates in the binary superacidic systems with the aim to isolate und structurally characterize salts containing a protonated carbonyl fluoride moiety.

[a] *S. Steiner, C. Jessen, A. J. Kornath*
Department Chemie, Ludwig-Maximilians-Universität München, Butenandtstraße 5–13, 81377 Munich, Germany
E-mail: andreas.kornath@cup.uni-muenchen.de
Homepage: http://www.org.chemie.uni-muenchen.de/ac/kornath

Supporting information for this article is available on the WWW under https://doi.org/10.1002/zaac.202200060

Results and Discussion

Synthesis and Properties of $[CClH_2C(OX)F][MF_6]$ and $[CH_2FC(OX)F][MF_6]$ (X = H, D; M = As, Sb)

Acetyl fluoride was reacted in the binary superacidic system HF/MF_5 (M = As, Sb) to obtain the acetylium ion as hexafluoridoarsenate (**1**) and hexafluoridostibate (**2**) according to Equation 1. The protonated species of acetyl fluoride was not observed under these conditions. The low temperature Raman and Infrared (IR) spectra of (**1**-**2**) and the starting material are illustrated in the Supporting Information (Figure S1 and Table S1).

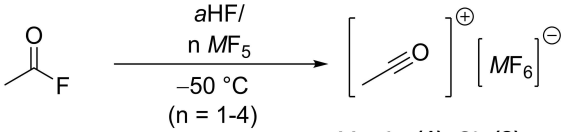

(1)

M = As **(1)**, Sb **(2)**

In order to study the influence of electron withdrawing groups on the Brønsted basicity of the acetyl fluorides, chloroacetyl fluoride and fluoroacetyl fluoride were reacted in the superacidic systems HF/MF_5 and DF/MF_5 (M = As, Sb).

The Lewis acid and anhydrous hydrogen fluoride or deuterium fluoride, respectively, were condensed into a FEP tube reactor. To form the superacid, both components were mixed at −50 °C. After the respective acetyl fluoride was condensed into the reaction vessel at −196 °C, the mixture was

warmed to −50 °C and the remaining HF was removed in dynamic vacuum. *O*-monoprotonated species of chloroacetyl fluoride and fluoroacetyl fluoride were obtained as hexafluoridoarsenates (**3**, **5**, **7**, **9**) and hexafluoridostibates (**4**, **6**, **8**, **10**) in quantitative yields as colorless solids, as presented in Equations 2 and 3.

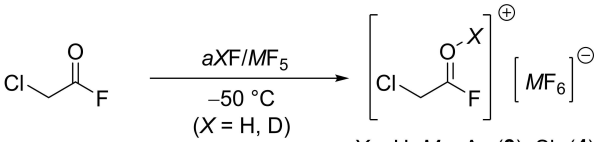

(2)

X = H: *M* = As (**3**), Sb (**4**)
X = D: *M* = As (**5**), Sb (**6**)

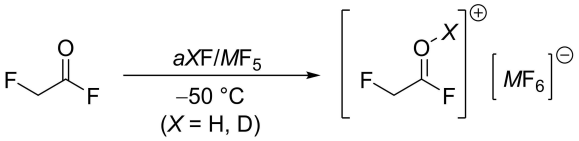

(3)

X = H: *M* = As (**7**), Sb (**8**)
X = D: *M* = As (**9**), Sb (**10**)

The hexafluoridoarsenates show thermal decomposition at −50 °C, the hexafluoridostibates at −30 °C.

Vibrational Spectroscopy

The low temperature Raman and IR spectra of $[CClH_2C(OX)F][AsF_6]$ (3, 5) (*X* = H, D) and $CClH_2COF$ are illustrated in Figure 1, the vibrational spectra of $[CH_2FC(OX)F][AsF_6]$ (7, 9) (*X* = H, D) and CH_2FCOF in Figure 2. In Table 1 and Table 2 selected observed Raman and IR frequencies of **3**, **4**, **7** and **8** are listed together with the quantum chemically calculated frequencies

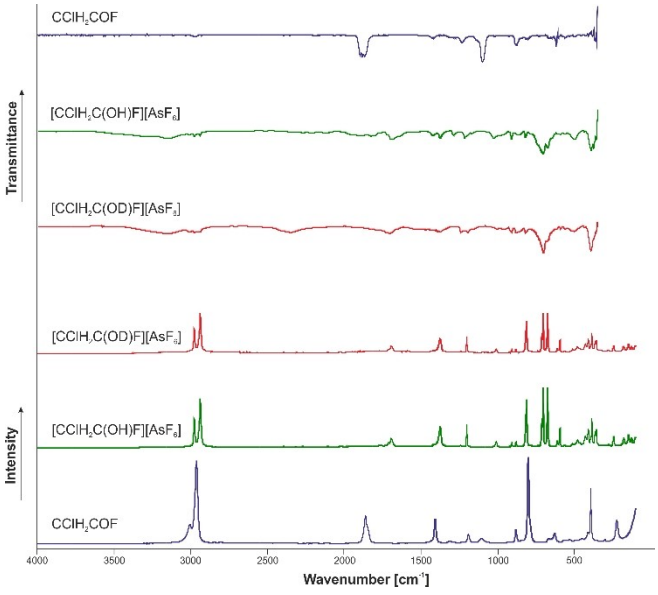

Figure 1. Low temperature Raman and IR spectra of $[CClH_2C(OX)F][AsF_6]$ (3, 5) (*X* = H, D) and $CClH_2COF$.

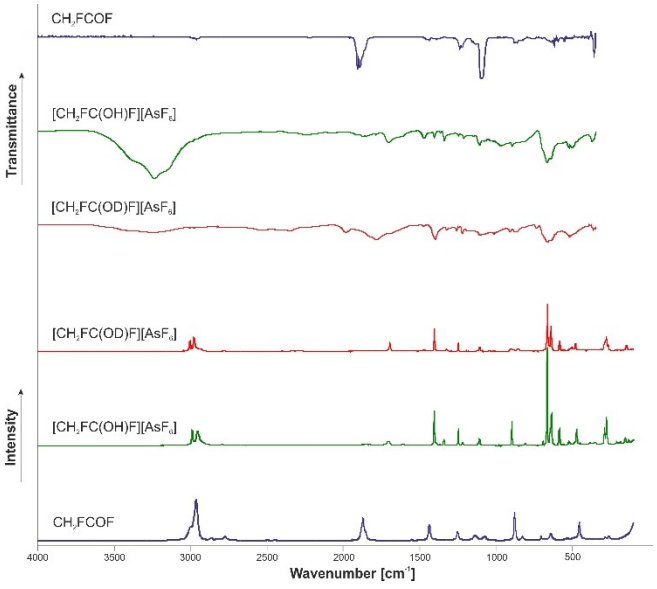

Figure 2. Low temperature Raman and IR spectra of $[CH_2FC(OX)F][AsF_6]$ (7, 9) (*X* = H, D) and CH_2FCOF.

of the HF-complexed cations $[CClH_2C(OH)F]^+ \cdot HF$ and $[CH_2FC(OH)F]^+ \cdot HF$ as well as their assignments. Hydrogen bonding between cation and anion has notable influence on the structure of the cations. Therefore, more suitable calculated vibrational frequencies were derived from adding a HF molecule to the calculation of the cations in the gas phase. These are discussed in the theoretical section below. The complete tables and the observed vibrational frequencies of the hexafluoridostibates (**4**, **6**) and (**8**, **10**) as well as of the analogue *D*-isotopomeric species and the starting materials are provided in the Supporting Information (Figures S2–S3 and Tables S2–S5).

Vibrational Spectra of $[CClH_2C(OX)F][AsF_6]$ (3, 5) and $[CClH_2C(OX)F][SbF_6]$ (4, 6) (X = H, D)

For the $[CClH_2C(OH)F]^+$ cation with C_1 symmetry 18 fundamental vibrational modes are expected, with all being Raman and IR active. The *ν*(O–H) vibration is overlaid by condensed water in the IR spectra due to the measuring method. Furthermore, the stretching vibration shows low intensity in the Raman spectra due to poor polarizability of the O–H group, which does not apply for the O–D group. The O–D stretching vibration of the *D*-isotopomeric species is significantly red-shifted to 2307 cm^{-1}, respectively 2308 cm^{-1} in the Raman spectra and to 2347 cm^{-1}, respectively 2341 cm^{-1} in the IR spectra. The isotopic shifts are in good agreement with the Teller-Redlich rule for an H/D isotopic effect.[8] The C=O stretching vibration is detected at 1695 cm^{-1} and is significantly red-shifted by approximately 160 cm^{-1} compared to the corresponding vibration of the starting material. The C–F stretching vibration occurs blue-shifted at 1190 cm^{-1}. Additionally, the *ν*(C–C) vibration is detected at around 900 cm^{-1} and thus blue-shifted by approx-

Table 1. Selected experimental vibrational frequencies [cm^{-1}] of $CClH_2COF$, $[CClH_2C(OH)F][AsF_6]$ (3) and $[CClH_2C(OH)F][SbF_6]$ (4) and calculated vibrational frequencies [cm^{-1}] of $[CClH_2C(OH)F]^+ \cdot HF$.

$CClH_2COF$ Raman	IR	$[CClH_2C(OH)F][AsF_6]$ (3) Raman	IR	$[CClH_2C(OH)F][SbF_6]$ (4) Raman	IR	$[CClH_2C(OH)F]^+ \cdot HF$ calc.[a,b] (IR/Raman)[c]	Assignment		
						2909(1404/34)	ν_3	A	ν(O–H)
1859(32)	1867 vs	1694(16)	1691 s	1692(5)	1691 w	1652(275/7)	ν_4	A	ν(C=O)
1105(6)	1097 vs	1200(39)	1213 s	1192(14)	1194 w	1187(104/1)	ν_8	A	ν(C–F)
880(16)	876 s	907(10)	908 s	909(10)	908 w	892(23/1)	ν_{11}	A	ν(C–C)
801(100)	798 m	812(79)	818 s	815(38)	814 m	803(37/9)	ν_{13}	A	ν(C–Cl)

[a] Calculated at the ωB97XD/aug-cc-pVTZ-level of theory, [b] Frequencies are scaled with a factor of 0.956, [c] IR intensity in [kJ/mol] und Raman intensity in [$Å^4$/a]. Abbreviations for IR intensities: vs = very strong, s = strong, m = medium, w = weak.

Table 2. Selected experimental vibrational frequencies [cm^{-1}] of CH_2FCOF, $[CH_2FC(OH)F][AsF_6]$ (7) and $[CH_2FC(OH)F][SbF_6]$ (8) and calculated vibrational frequencies [cm^{-1}] of $[CH_2FC(OH)F]^+ \cdot HF$.

CH_2FCOF Raman	IR	$[CH_2FC(OH)F][AsF_6]$ (7) Raman	IR	$[CH_2FC(OH)F][SbF_6]$ (8) Raman	IR	$[CH_2FC(OH)F]^+ \cdot HF$ calc.[a,b] (IR/Raman)[c]	Assignment		
						2874(2052/40)	ν_2	A′	ν_s(O–H)
1871(53)	1890 s	1697(22)	1692 w	1699(19)	1701 w	1667(298/7)	ν_3	A′	ν_s(C=O)
1074(10)	1095 vs			1221(4)	1212 w	1208(103/1)	ν_7	A′	ν_s(C–F)
1139(13)	1132 w	1112(7)	1105 m	1104(10)	1107 m	1144(105/3)	ν_8	A′	$\nu_s(C_{H2}–F)$
828(10)	824 w	898(33)	897 w	897(39)	895 m	857(15/5)	ν_9	A′	ν_s(C–C)

[a] Calculated at the ωB97XD/aug-cc-pVTZ-level of theory, [b] Frequencies are scaled with a factor of 0.956, [c] IR intensity in [kJ/mol] und Raman intensity in [$Å^4$/a]. Abbreviations for IR intensities: vs = very strong, s = strong, m = medium, w = weak.

imately 30 cm^{-1} in comparison to chloroacetyl fluoride. The observed shifts are consistent with the elongation of the C=O bond and the shortening of the C–F as well as C–C bonds due to protonation (see crystallographic section below). The C–Cl stretching vibration as well as the C–H stretching and CH_2 bending vibrations of the salts (**3**, **4**, **5**, **6**) are not affected by the protonation. For the anions $[AsF_6]^-$ and $[SbF_6]^-$ with octahedral symmetry more vibrations are observed than expected due to interionic interactions in the solid leading to a symmetry distortion.

Vibrational Spectra of $[CH_2FC(OX)F][AsF_6]$ (7, 9) and $[CH_2FC(OX)F][SbF_6]$ (8, 10) (X = H, D)

For the $[CH_2FC(OH)F]^+$ cation with C_S symmetry, 18 fundamental vibrational modes are expected, with all being Raman and IR active.

The O–D stretching vibrations occur substantially red-shifted at 2307 cm^{-1} and 2285 cm^{-1} in the Raman spectra and at 2353 cm^{-1} and 2347 cm^{-1} in the IR spectra and are in good agreement with the Teller-Redlich rule for a H/D isotopic effect.[8] Analogous to the protonated chloroacetyl fluoride, the C=O stretching vibration occurs significantly red-shifted by approximately 175 cm^{-1} compared to the starting material at around 1700 cm^{-1} and confirms the *O*-monoprotonation of the carbonyl group.

Further, the ν_s(C–F) vibration is detected at around 1220 cm^{-1}, hence shifted towards higher wavenumbers by approximately 50 cm^{-1}. In comparison to the protonated species of chloroacetyl fluoride (1190 cm^{-1}), the C–F stretching vibration is slightly blue-shifted. The ν_s(C–C) vibration appears blue-shifted at around 900 cm^{-1}.

All observed shifts are consistent with the elongation of the C=O bond and the shortening of the C–F bond due to protonation (see crystallographic section below).

The C–F stretching vibration of the fluoromethyl group as well as the C–H stretching and CH_2 bending vibrations of the salts (**7**, **8**, **9**, **10**) are not affected by protonation. For the octahedral anions $[AsF_6]^-$ and $[SbF_6]^-$ more vibrations are observed than expected, due to solid-state effects leading to a lowered symmetry.

Crystal Structures

Crystal Structure of $[CClH_2C(OH)F][SbF_6]$ (4)

The hexafluoridostibate of monoprotonated chloroacetyl fluoride (**4**) crystallizes in the monoclinic space group $P2_1/c$ with four formula units per unit cell. The asymmetric unit of **4** is illustrated in Figure 3. Crystal data and structure refinement are provided in the Supporting Information (Table S6). Selected structural parameters are listed in Table 3 in comparison to geometric data of the starting material[9] and theoretical calculations.

Due to protonation the C=O bond (1.231(3) Å) is elongated compared to the starting material (1.183 Å) and therefore,

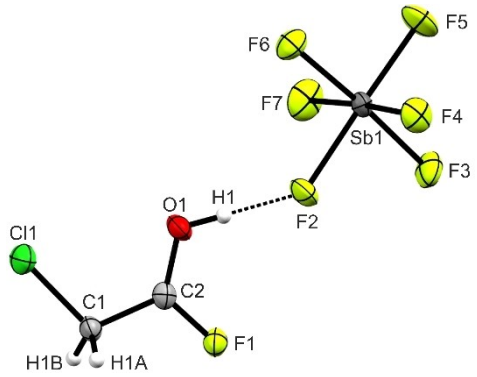

Figure 3. Asymmetric unit of **4** (displacement ellipsoids with 50% probability).

Table 3. Selected bond lengths [Å] and bond angles [°] of $CClH_2COF$ (Cl*Ac*F), $[CClH_2C(OH)F][SbF_6]$ (4) and the calculated $[CClH_2C(OH)F]^+ \cdot HF$ as well as donor-acceptor distances in **4**. Symmetry codes: *i* = −*x*, 1−*y*, 1−*z*; *ii* = 1−*x*, −0.5 + *y*, 1.5−*z*; *iii* = 1 + *x*, 1.5−*y*, 0.5 + *z*.

	Cl*Ac*F[9]*	**4**	$[CClH_2C(OH)F]^+ \cdot HF$[a]
Bond lengths [Å]			
C1–Cl1	1.763	1.753(3)	1.749
C1–C2	1.506	1.469(4)	1.478
C2–O1	1.183	1.231(3)	1.238
C2–F1	1.324	1.285(3)	1.277
Bond angles [°]			
Cl1–C1–C2	113.2	112.4(2)	113.9
C1–C2–O1	130.1	124.2(2)	124.5
C1–C2–F1	108.1	116.4(2)	116.4
F1–C2–O1		119.4(2)	119.1
Dihedral angles [°]			
Cl1–C1–C2–O1		6.4(4)	−0.0
Cl1–C1–C2–F1		−174.2(2)	180.0
Donor-acceptor distances [Å]			
O1–(H1)···F2	2.421(3)	C1–(H1B)···F3*ii*	3.029(4)
C1–(H1A)···F4*i*	3.048(3)	C2···F4*i*	2.704(3)
C1–(H1A)···F7*iii*	3.141(3)	C2···F5*ii*	2.651(3)

[a] Calculated at the ωB97XD/aug-cc-pVTZ-level of theory. * No standard uncertainties mentioned.

longer than a formal C=O double bond (1.19 Å).[3] Furthermore, the bond length C2–F1 (1.285(3) Å) is shortened in comparison to the neutral compound (1.324 Å) and a formal C–F bond (1.36 Å).[3] The same applies for the bond length C1–C2 (1.469(4) Å) (starting material 1.506 Å). The $[CClH_2C(OH)F]^+$ cation possesses a nearly planar carbonyl fluoride moiety. The bond angle C2–C1–O1 (124.2(2)°) is decreased by approximately 6° by protonation (130.1°). The Sb–F bond lengths are in the range between 1.856(2) Å and 1.923(2) Å and correspond with values reported in the literature.[10–12] Due to interionic interactions the anion displays slightly distorted octahedral symmetry. The Sb1–F2 bond is significantly longer than the other Sb–F bonds with it being involved in hydrogen bonding.

In the crystal structure of **4** the cations and anions are linked by the strong hydrogen bond O1–(H1)···F2 (according to the classification by *Jeffrey*).[13] The C···F interaction C2···F4*i* leads to formation of cation-anion pairs, which are linked by the interaction C2···F5*ii* and distorted by 90° to each other (see Figure 4 and S4). The fluorine bridges contribute to enhanced stabilization of the positive charge located at the carbonyl carbon. Interatomic distances are listed in Table 3.

Crystal Structure of $[CH_2FC(OD)F][SbF_6]$ (10)

The hexafluoridostibate of monoprotonated fluoroacetyl fluoride (**10**) crystallizes in the triclinic space group $P\bar{1}$ with two formula units per unit cell. The asymmetric unit of **10** is illustrated in Figure 5. Crystal data and refinement are provided in the Supporting Information (Table S6). Selected structural parameters are listed in Table 4 together with structural parameters of the starting material[15] and theoretical calculations.

Analogous to chloroacetyl fluoride, protonation leads to significant elongation of the bond length C1–O1 (1.227(5) Å) compared to the neutral compound (1.194(13) Å). The bond length C1–F1 (1.278(4) Å) is significantly shortened in comparison to fluoroacetyl fluoride (1.351(14) Å) and is also shorter than the C–F bond of the *O*-monoprotonated species of chloroacetyl fluoride (1.286(3) Å). The $[CH_2FC(OD)F]^+$ cation consists of a nearly planar carbonyl fluoride moiety. Due to protonation, the bond angle C2–C1–O1 (123.3(3)°) is decreased by approximately 6° (129.9(7)°).

The Sb–F bond lengths are in the range between 1.854(2) Å and 1.929(2) Å and correspond with values reported in the literature.[10–12] Due to solid-state effects the anion displays

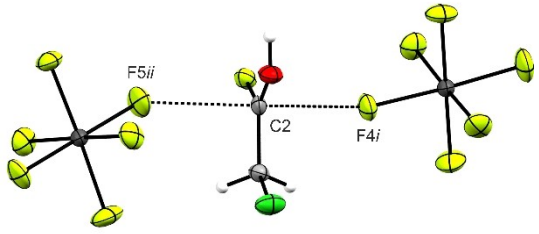

Figure 4. Layer structure of **4** (displacement ellipsoids with 50% probability). Symmetry codes: *i* = −x, 1-y, 1-z; *ii* = 1-x, −0.5 + y, 1.5-z.

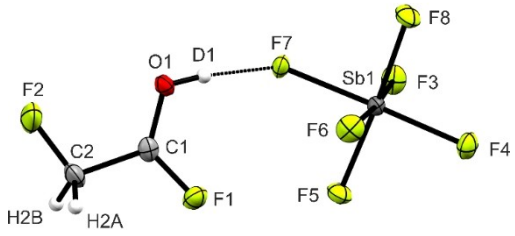

Figure 5. Asymmetric unit of 10 (displacement ellipsoids with 50% probability).

Table 4. Selected bond lengths [Å] and bond angles [°] of CH_2FCOF (F*Ac*F), $[CH_2FC(OD)F][SbF_6]$ (10) and the calculated $[CH_2FC(OH)F]^+ \cdot HF$ as well as donor-acceptor distances in **10**. Symmetry codes: $i = 1-x, 1-y, 1-z$.

	F*Ac*F[15]	**10**	$[CH_2FC(OH)F]^+ \cdot HF$[a]
Bond lengths [Å]			
C2–F2	1.366(7)	1.359(5)	1.341
C2–C1	1.483(7)	1.484(5)	1.490
C1–O1	1.194(13)	1.227(5)	1.236
C1–F1	1.351(14)	1.278(4)	1.274
Bond angles [°]			
F2–C2–C1	110.3(5)	108.9(3)	110.3
C2–C1–O1	129.9(7)	123.2(3)	122.9
C2–C1–F1	109.6(10)	115.8(3)	116.9
F1–C1–O1		121.0(3)	120.2
Dihedral angles [°]			
F2–C2–C1–O1		0.1(5)	0.0
F2–C2–C1–F1		−179.0(3)	−180.0
Donor-acceptor distances [Å]			
O1–(D1)···F7	2.465(3)	C1···F3*i*	2.618(4)
C2–(H2A)···F8	3.113(4)	C1···F6*i*	2.622(4)
C2–(H2B)···F4*i*	3.219(4)		

[a] Calculated at the ωB97XD/aug-cc-pVTZ-level of theory.

slightly distorted octahedral symmetry. The Sb1–F7 bond is significantly longer than the other Sb–F bonds with it being involved in hydrogen bonding.

In the crystal structure of **10** the cations and anions are arranged in chains along the *a*-axis by the strong hydrogen bond O1–(D1)···F7 and the weak hydrogen bond C2–(H2 A)···F8.[13] Layers are formed by antiparallel chains connected by the C···F interactions C1···F3*i* and C1···F6*i* (Figure 6),[14] which contribute to the stabilization of the positive charge localized at the carbonyl carbon. The layers are linked by the weak hydrogen bond C2–(H2B)···F4*i*. Interatomic distances are listed in Table 4.

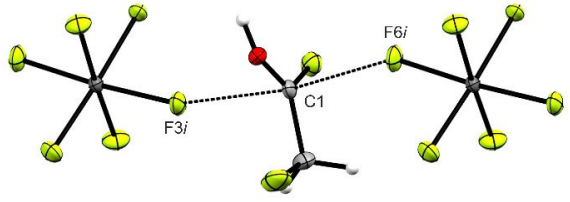

Figure 6. Layer structure of **10** (displacement ellipsoids with 50% probability). Symmetry codes: $i = 1-x, 1-y, 1-z$.

Table 5. Selected ^{13}C and ^{19}F NMR chemical shifts [ppm] and $^1J_{C-F}$ coupling constants [Hz] of Cl*Ac*F, $[CClH_2C(OH)F][SbF_6]$ (4), F*Ac*F and $[CH_2FC(OH)F][SbF_6]$ (8).

	Cl*Ac*F	**4**	F*Ac*F	**8**
δ ^{19}F obs [ppm], C(OH)**F**	31.52 (s)	46.60 (s)	20.46 (d)	30.02 (d)
δ ^{13}C obs [ppm], **C**(OH)F	164.5 (d)	190.1 (d)	165.1 (d)	188.5 (dd)
$^1J_{C-F}$ [Hz]	358.0	379.7	359.6	363.7

NMR Spectroscopy

^1H, ^{19}F and ^{13}C NMR spectra of the monoprotonated species **4** and **8** as well as the neutral compounds dissolved in *a*HF were measured at −50 °C. In Table 5 selected observed NMR shifts and coupling constants are summarized. The measured NMR spectra and the complete NMR data of **4**, **8** and the starting materials are listed in the Supporting Information (Figures S5–S9).

The ^{19}F NMR spectrum of **4** shows a singlet of the carbonyl fluorine at 46.60 ppm and consequently the ^{13}C NMR spectrum of **4** displays a doublet of the carbonyl carbon at 190.1 ppm. The $^1J_{C-F}$ coupling constant is 379.7 Hz. Due to replacement of the chlorine atom by fluorine, the NMR resonances of the carbonyl fluorine in the ^{19}F NMR spectrum of **8** as well as of the carbonyl carbon in the ^{13}C NMR spectrum are both shifted upfield. A doublet is located at 30.02 ppm for the carbonyl fluorine in the ^{19}F NMR spectrum and a doublet of doublets at 188.5 ppm for the carbonyl carbon in the ^{13}C NMR spectrum, respectively. Further, the $^1J_{C-F}$ coupling constant is slightly decreased to 363.7 Hz. The magnitude of both $^1J_{C-F}$ coupling constants corresponds with values reported in the literature, found for one-bond ^{13}C–^{19}F coupling constants of fluorine-substituted carbenium ions.[16–17]

Compared to neutral compounds, the NMR resonances of the *COF* moieties of both monoprotonated species **4** and **8** are shifted downfield significantly in the ^{19}F NMR and ^{13}C NMR spectra.

Theoretical Calculations

The quantum chemical calculations were performed at the ωB97XD/aug-cc-pVTZ-level of theory at 298 K with the Gaussian16 program package.[18] Solid-state effects and intermolecular interactions, especially the hydrogen bonding between the cation and anion, have notable influence on the structure of the cations. Thus, the hydrogen bonds were simulated by adding an additional HF molecule to the cation in the gas phase leading to more suitable results, in particular with regard to the carbonyl bond and the calculated vibrational frequencies. This method is already established in the literature.[19]

In Figure 7, the calculated cations are illustrated with selected bond lengths and angles in comparison to the crystal structures. The calculated values of the cations are in good agreement with the experimentally obtained data.

As observed in the single-crystal X-ray structures, protonation causes a significant elongation of the carbonyl bond and a significant shortening of the C–F bond. Mapped Electrostatic Potentials (MEPs) were calculated together with Natural Population Analysis charges (NPAs) to gain insight into the bonding situation in the carbonyl fluoride moiety. Figure 8, Figure 9 and Figure 10 depict the MEPs together with the NPAs of

Journal of Inorganic and General Chemistry
ZAAC
Zeitschrift für anorganische und allgemeine Chemie

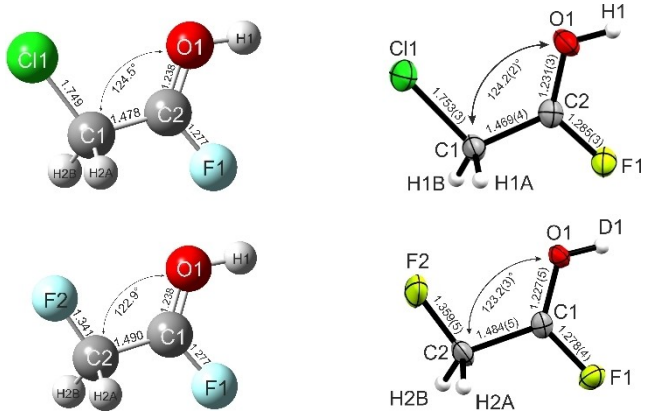

Figure 7. Calculated gas phase structures of $[CClH_2C(OH)F]^+$ and $[CH_2FC(OH)F]^+$ and the cations derived from the X-ray structures (4) and (10).

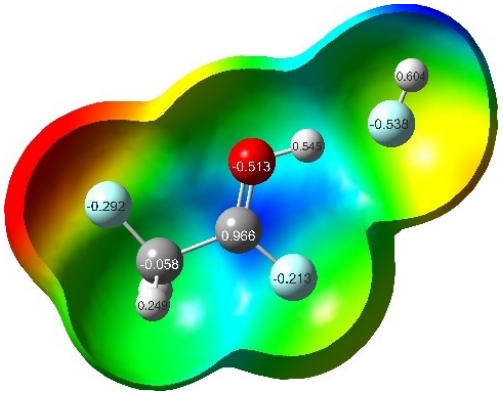

Figure 10. Molecular 0.0004 $bohr^{-3}$ 3D isosurfaces with mapped electrostatic potential as a color scale ranging from 0.11 a.u. (red) to 0.23 (blue). The electrostatic potential isosurfaces and the NPA charges have been calculated for $[CH_2FC(OH)F]^+ \cdot HF$.

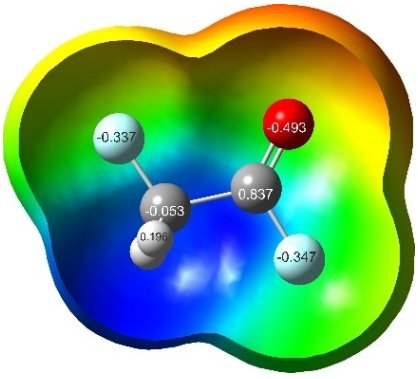

Figure 8. Molecular 0.0004 $bohr^{-3}$ 3D isosurfaces with mapped electrostatic potential as a color scale ranging from −0.04 a.u. (red) to 0.04 (blue). The electrostatic potential isosurfaces and the NPA charges have been calculated for CH_2FCOF.

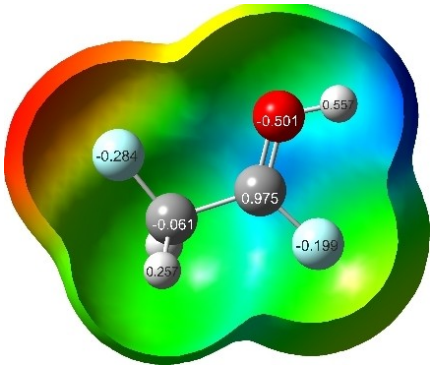

Figure 9. Molecular 0.0004 $bohr^{-3}$ 3D isosurfaces with mapped electrostatic potential as a color scale ranging from 0.11 a.u. (red) to 0.27 (blue). The electrostatic potential isosurfaces and the NPA charges have been calculated for $[CH_2FC(OH)F]^+$.

fluoroacetyl fluoride, $[CH_2FC(OH)F]^+$ and $[CH_2FC(OH)F]^+ \cdot HF$. According to the calculations, the positive electrostatic potential (blue) in the starting material is located at the two neighboring carbon atoms, whereas the negative electrostatic potential (red) is located at the fluorine and oxygen atoms. Comparing the NPA charges of fluoroacetyl fluoride and the protonated species, the positive charge on the carbonyl carbon increases due to protonation and leads to higher electrophilicity of the carbonyl fluoride moiety. This can be affirmed by the formation of C···F interactions in the crystal structures, which contribute to enhanced stabilization of the positive charge, as well as the high positive electrostatic potential on the MEPs of the protonated species. The addition of a HF molecule for the simulation of the hydrogen bonding in the solid-state results in even stronger localization of the positive charge on the carbonyl carbon.

Whilst the negative charge on the oxygen slightly increases due to protonation, it strongly decreases for the carbonyl fluorine. This leads to the assumption, that the positive charge located at the carbon is stabilized due to electron-donating effects of the fluorine.

The concept of stabilization of carbocations by halogen substituents, especially fluorine atoms bound to the cationic centers is well investigated. It was found for fluorine-substituted carbenium ions that electron donation of fluorine lone-pair orbitals into the formally empty p(π) atom orbital of the carbons can stabilize electron deficient cationic centers, despite fluorine being the most electronegative element.[16,17,20–22]

This prompted us to perform NBO calculations to gain a more detailed insight into the protonated *COF* moiety. Our intention was to investigate if similar interactions occur for both protonated haloacetyl fluorides. In case of fluoroacetyl fluoride we found that the p-orbital of fluorine is occupied by 1.900 e and the σ*(C–F) orbital by 0.147 e, respectively. The π*(C=O) orbital is occupied by 0.137 e. Due to *O*-monoprotonation, occupation of the $p_{(F)}$-orbital and σ*(C–F) orbital is lowered to 1.838 e and 0.056 e, respectively, whereas the occupation of the π*(C=O) orbital is increased to 0.241 e. Further, a strong $p_{(F)}$-π*(C=O) interaction was found, indicating that fluorine signifi-

cantly stabilizes the positive charge located at the carbonyl carbon through back-donation of lone-pair electrons, resulting in a strengthening of the C–F bond as well as a blue-shift of the *ν*(C–F) in the vibrational spectra, as mentioned above.

The influence of substituents on fluorine back-donation was investigated by *Olah et al.* with NMR spectroscopy.[16,17] It was found that one-bond $^{13}C–^{19}F$ coupling constants can be used as criteria to measure the extend of fluorine back-donation. Thus, electron-withdrawing substituents increase the electron demand of the cationic center, which results in increased back-donation and an increased $^{13}C–^{19}F$ coupling constant. Further, the ^{19}F and ^{13}C NMR resonances are shifted downfield in comparison to the corresponding resonances with electron donating substituents. In case of substitution by chlorine and fluorine, analog trends were observed as in case of the protonated species of chloroacetyl fluoride and fluoroacetyl fluoride.[16,17] Therefore, increased electron demand of the carbonyl carbon due to fluorine substitution leads to a decrease of the $^{1}J_{C\text{-}F}$ coupling constant compared to the chloro-analogue. The almost identical ^{13}C NMR shifts of the carbonyl carbons indicate compensation and stabilization of the positive charges through back-donation of fluorine lone-pair electrons.

The MEPs of chloroacetyl fluoride and the corresponding cations together with the NPAs are illustrated in the Supporting Information (Figure S11–S13). Here, results similar to those of fluoroacetyl fluoride were found.

Conclusion

Acetyl fluoride was reacted in the binary superacidic system HF/MF_5 (M = As, Sb) under formation of acetylium salts. A protonated species was not observed and could not be isolated.

Unlike acetyl fluoride, chloroacetyl fluoride and fluoroacetyl fluoride were *O*-monoprotonated in the binary superacidic systems HF/MF_5 and DF/MF_5 (M = As, Sb). Thus, substitution of the methyl group with electron-withdrawing atoms such as chlorine or fluorine enables the preparation of the protonated species as well as the haloacetylium ions, depending on using superacidic or Lewis-acidic reaction conditions.

The colorless salts were characterized by low-temperature vibrational spectroscopy, low-temperature NMR spectroscopy and single-crystal X-ray diffraction analyses. The experimental data are discussed together with quantum chemical calculations at the ωB97XD/aug-cc-pVTZ-level of theory. NBO calculations were performed alongside calculations of Mapped Electrostatic Potentials and Natural Population Analysis charges to confirm an increase of the electrophilicity of the carbonyl carbon and stabilization of the positive charge through fluorine lone-pair electron back-donation, resulting in the elongation of the carbonyl bond and shortening of the C–F bond as well as a red-shift of the C=O stretching vibration and a blue-shift of the *ν*(C–F) in the vibrational spectra.

Experimental Section

Caution! Avoid skin contact with all compounds. Hydrolysis can lead to formation of HF or DF that burns skin and causes irreparable damage. Ensure appropriate safety precautions while handling these materials.

Apparatus and Materials: All reactions were performed employing standard Schlenk techniques using a stainless-steel vacuum line. Syntheses were carried out using FEP/PFA tube-reactors closed with stainless-steel valves. Prior to use, the stainless-steel vacuum line and all reactors were dried with fluorine. Low temperature Raman spectra were recorded under vacuum using glass cells cooled with liquid nitrogen and a Bruker® MultiRAMII FT Raman spectrometer equipped with Nd:YAG laser (λ = 1064 nm) and a laser excitation of 500–1000 mW. Low temperature IR spectra were recorded with a Bruker® Vertex FT IR spectrometer at −196 °C. For measurements, low temperature IR cells[23] were prepared with CsBr single-crystal plates coated with a small amount of the samples. For visualization the software Advanced Chemistry Development Inc.® (ACD/Labs 2015) was employed. Low temperature X-ray diffraction was performed with an Oxford XCalibur3 diffractometer equipped with a Spellman Generator (50 kV, 40 mA) and a Kappa CCD detector, using Mo-Kα radiation (λ = 0.71073 Å). The program CrysAlisPro 1.171.38.46 (Rigaku OD, 2015)[24] was employed for the data collection and reduction. The structure solution and refinement were performed with the software SHELXT[25] and SHELXL-2018/3,[26] implemented in the WinGX software package.[27] The solution was checked with the program PLATON[28] and the absorption correction was performed using the SCALE3 ABSPACK multi-scan-method.[29] Selected data and parameters of the single-crystal X-ray structure analyses are summarized in Table S6 for **4** and **10**, respectively (see Supporting Information). Crystallographic data (excluding structure factors) for the structures in this paper were deposited with the Cambridge Crystallograpic Data Centre, CCDC, 12 Union Road, Cambridge CB21EZ, UK. Copies of the data can be obtained free of charge on quoting the depository number CCDC-2023176 for $[CClH_2C(OH)F][SbF_6]$ (**4**) and CCDC-2023175 for $[CHF_2C(OH)F][SbF_6]$ (**10**) (Fax: +44-1223-336-033; E-Mail: deposit@ccdc.cam.ac.uk, http://www.ccdc.cam.ac.uk). NMR samples were prepared by adding the HF solution to a small FEP tube under nitrogen stream. The tube was sealed under vacuum and inserted into a standard NMR tube. For ^{1}H, ^{19}F and ^{13}C NMR measurements a Bruker AV400TR and a JEOL ECX 400 NMR spectrometer were used. For evaluation MNOVA by Mestrelab was used.[30] Quantum chemical calculations were performed at the ωB97XD/aug-cc-pVTZ-level of theory by Gaussian16.[18] GaussView 6.0 was used for visualization and illustration of the MEP calculations.[31]

Typical Procedure (TP1); Synthesis of *O*-monoprotonated haloacetyl fluorides using superacidic system HF/MF_5 (M = As, Sb): The Lewis acid and anhydrous hydrogen fluorine were condensed into a FEP tube-reactor at −196 °C. To form the superacid, the mixture was warmed to −50 °C and both components were mixed. After the mixture was cooled to −196 °C again, the haloacetyl fluoride was condensed into the reaction vessel. Subsequently, the mixture was warmed to −50 °C and all components were reacted. Then, the temperature was reduced to −78 °C. The remaining HF was removed in dynamic vacuum at −78 °C. The salts were obtained in quantitative yield as colorless solids.

Synthesis of $[CClH_2C(OH)F][AsF_6]$: Compound **(3)** was prepared from arsenic pentafluoride (1 mmol, 170 mg, 1.0 eq.), anhydrous hydrogen fluoride (100 mmol, 2 mL), and chloroacetyl fluoride (1 mmol, 96 mg, 1.0 eq.) as described in TP1. Compound **(5)** was prepared analogously, using *a*DF instead of *a*HF.

Synthesis of $[CClH_2C(OH)F][SbF_6]$: Compound **(4)** was prepared from antimony pentafluoride (1 mmol, 217 mg, 1.0 eq.), anhydrous hydrogen fluoride (100 mmol, 2 mL), and chloroacetyl fluoride (1 mmol, 96 mg, 1.0 eq.) as described in TP1. Compound **(6)** was prepared analogously, using *a*DF instead of *a*HF.

Synthesis of $[CH_2FC(OH)F][AsF_6]$: Compound **(7)** was prepared from arsenic pentafluoride (1 mmol, 170 mg, 1.0 eq.), anhydrous hydrogen fluoride (100 mmol, 2 mL), and fluoroacetyl fluoride (1 mmol, 80 mg, 1.0 eq.) as described in TP1. Compound **(9)** was prepared analogously, using *a*DF instead of *a*HF.

Synthesis of $[CH_2FC(OH)F][SbF_6]$: Compound **(8)** was prepared from antimony pentafluoride (1 mmol, 217 mg, 1.0 eq.), anhydrous hydrogen fluoride (100 mmol, 2 mL), and fluoroacetyl fluoride (1 mmol, 80 mg, 1.0 eq.) as described in TP1. Compound **(10)** was prepared analogously, using *a*DF instead of *a*HF.

Acknowledgements

We are grateful to the Department of Chemistry of the Ludwig Maximilian University, the Deutsche Forschungsgemeinschaft (DFG) and F-Select GmbH for the financial support of this work. Open Access funding enabled and organized by Projekt DEAL.

Conflict of Interest

The authors declare no conflict of interest.

Data Availability Statement

The data that support the findings of this study are available in the supplementary material of this article.

Keywords: acetyl fluoride · chloroacetyl fluoride · fluoroacetyl fluoride · superacid · protonation · structure elucidation · fluorine back-donation

[1] C. Waschke, H. G. Roskos, R. Schwedler, K. Leo, H. Kurz, K. Köhler, *Phys. Rev. Lett.* **1993**, *70*, 3319.
[2] J. A. Hyatt, P. W. Raynolds, *J. Org. Chem.* **1984**, *49*, 384–385.
[3] A. F. Holleman, E. Wiberg, N. Wiberg, *Anorganische Chemie*, De Gruyter, Berlin, Boston, **2017**.
[4] F. Seel, *Z. Anorg. Allg. Chem.* **1943**, *252*, 24–26.
[5] G. A. Olah, A. Germain, H. C. Lin, *J. Am. Chem. Soc.* **1975**, *97*(19), 5481–5488.
[6] G. A. Olah, M. B. Comisarow, *J. Am. Chem. Soc.* **1966**, *88*, 4442–4447.
[7] A. Commeyras, G. A. Olah, *J. Am. Chem. Soc.* **1969**, *91*(11), 2929–2942.
[8] J. Weidlein, U. Müller, K. Dehnicke, *Schwingungsspektroskopie, Vol. 2nd ed.*, Georg Thieme Verlag, Stuttgart, Germany, **1988**.
[9] B. P. van Eijck, V. M. Stolwijk, *J. Mol. Spectrosc.* **1985**, *111*, 164–172.
[10] R. Minkwitz, N. Hartfeld, C. Hirsch, *Z. Anorg. Allg. Chem.* **1999**, *625*, 1479.
[11] R. Minkwitz, S. Schneider, *Angew. Chem. Int. Ed.* **1999**, *38*, 210.
[12] R. Minkwitz, C. Hirsch, T. Berends, *Eur. J. Inorg. Chem.* **1999**, *1999*(12), 2249.
[13] G. A. Jeffrey, *An introduction to hydrogen bonding*. Topics in physical chemistry, Oxford Univ. Press, New York, **1997**.
[14] A. Bondi, *J. Phys. Chem.* **1964**, *68*, 441.
[15] B. P. van Eijck, P. Brandts, J. P. M. Maas, *J. Mol. Struct.* **1978**, *44*, 1–13.
[16] G. A. Olah, M. Stephenson, J. G. Shih, V. V. Krishnamurthy, G. K. S. Prakash, *J. Fluorine Chem.* **1988**, *40*, 319–329.
[17] G. K. S. Prakash, L. Heiliger, G. A. Olah, *J. Fluorine Chem.* **1990**, *49*, 33–41.
[18] M. J. Frisch, G. W. Trucks, H. B. Schlegel, G. E. Scuseria, M. A. Robb, J. R. Cheeseman, G. Scalmani, V. Barone, B. Mennucci, G. A. Petersson, H. Nakatsuji, M. Caricato, X. Li, H. P. Hratchian, A. F. Izmaylov, J. Bloino, G. Zheng, J. L. Sonnenberg, M. Hada, M. Ehara, K. Toyota, R. Fukuda, J. Hasegawa, M. Ishida, T. Nakajima, Y. Honda, O. Kitao, H. Nakai, T. Vreven, J. A. Montgomery, J. E. Peralta, F. Ogliaro, M. Bearpark, J. J. Heyd, E. Brothers, K. N. Kudin, V. N. Staroverov, R. Kobayashi, J. Normand, K. Raghavachari, A. Rendell, J. C. Burant, S. S. Iyengar, J. Tomasi, M. Cossi, N. Rega, J. M. Millam, M. Klene, J. E. Know, J. B. Cross, V. Bakken, C. Adamo, J. Jaramillo, R. Gomperts, R. E. Stratmann, O. Yazyev, A. J. Austin, R. Cammi, C. Pomelli, J. O. Ochterski, R. L. Martin, K. Morokuma, V. G. Zakrzweski, G. A. Voth, P. Salvador, J. J. Dannenberg, S. Dapprich, A. D. Daniels, O. Farkas, J. B. Foresman, J. V. Ortiz, J. Cioslowski, D. J. Fox, *Gaussian16, Revision C.01*, Gaussian Inc., Wallingford CT, **2016**.
[19] T. Soltner, N. Goetz, A. Kornath, *Eur. J. Inorg. Chem.* **2011**, *20*, 5429–5435.
[20] G. Frenking, W. Koch, H. Schwarz, *J. Comput. Chem.* **1986**, *7*(4), 406–416.
[21] K. O. Christe, X. Zhang, R. Bau, J. Hegge, G. A. Olah, G. K. S. Prakash, J. A. Sheehy, *J. Am. Chem. Soc.* **2000**, *122*, 481–487.
[22] G. A. Olah, G. Liang, Y. K. Mo, *J. Org. Chem.* **1974**, *39*(16), 2394–2398.
[23] L. Bayersdorfer, R. Minkwitz, J. Jander, *Z. Anorg. Allg. Chem.* **1972**, *393*(2), 137–142.
[24] Rigaku Oxford Diffraction, CrysAlisPro Software System, *Version 1.171.38.46*, Rigaku Corporation, Oxford, UK, **2015**.
[25] G. M. Sheldrick, *Acta Crystallogr A Found Adv* **2015**, *71*, 3.
[26] G. M. Sheldrick, *Acta Crystallogr. Sect. C* **2015**, *71*, 3.
[27] L. J. Farrugia, *J. Appl. Crystallogr.* **1999**, *32*(4), 837–838.
[28] A. Spek, *PLATON, A Multipurpose Crystallographic Tool*, Utrecht University, Utrecht (The Netherlands), **1999**.
[29] *SCALE3 ABSPACK* – An Oxford Diffraction program, Oxford Diffraction Ltd. **2005**.
[30] MestReNova 14.0, Mestrelab Research, 2019.
[31] R. Dennington, T. A. Keith, J. M. Millam, *GaussView Version 6.0*, Semi-chem Inc. Shawnee Mission, KS, **2016**.

Manuscript received: February 10, 2022
Revised manuscript received: April 11, 2022
Accepted manuscript online: April 12, 2022

